Prediction of A_2BX_4 metal-chalcogenide compounds via first-principles thermodynamics

X. Zhang
Department of Physics, Colorado School of Mines, Golden, Colorado 80401, USA

V. Stevanović, M. d'Avezac, and S. Lany
National Renewable Energy Laboratory, Golden, Colorado 80401, USA

Alex Zunger*
University of Colorado, Boulder, CO 80309, USA

(Received 21 October 2011; revised manuscript received 5 January 2012; published 16 July 2012)

Current compilations of previously documented inorganic compounds reveal a significant number of materials that are not listed. Focusing on the A_2BX_4 metal-chalcogenide group with A and B atoms being either main group elements or only one of them being a $3d$ transition metal, a total of 255 are reported, whereas 429 chemically reasonable A_2BX_4 are unreported. We have applied first-principles thermodynamics based on density functional methodology, predicting that about 100 of the 429 unreported A_2BX_4 metal-chalcogenides are likely to be stable. These include 14 oxides, 34 sulfides, 28 selenides, and 24 tellurides that are predicted here to be energetically stable with respect to decomposition into any combination of elemental, binary, and ternary competing phases. We provide the lowest-energy crystal structures of the predicted A_2BX_4 compounds, as well as the next few energetically higher metastable structures. Such predictions are carried out via direct first-principles calculations of candidate structure types and confirmed for a few compounds using the global space-group optimization (GSGO) search method. In some cases, uncommon oxidation states and/or coordination environments are found for elements in the stable A_2BX_4 compounds predicted here. We estimated the growth conditions in terms of temperature and partial pressure of the reactants from extensive thermodynamic stability analysis, and found dozens of compounds that might be grown at normal synthesis conditions. Attempts at synthesis of the stable A_2BX_4 compounds predicted here are called for.

DOI: 10.1103/PhysRevB.86.014109 PACS number(s): 61.66.Fn, 61.50.Nw

I. INTRODUCTION

One of the remarkable aspects of semiconductor-based high-technology is the fact that such a broad range of electronic and optoelectronic devices are based on such a narrow base of active materials: constructed by the covalently bonded binary diamond-like and zinc-blende compounds, comprising in the order of ten individual base materials. Attempts to venture into completely different chemical and structural groups in search of relevant functionalities, such as semiconductivity, transparent conductivity, or solar absorbance, have recently been intensified in light of the accumulated knowledge on the technological limitation of the group of usual-suspects binary materials.[1] In this respect, the group of A_2BX_4 materials, with metallic A and B elements and X a chalcogen (O, S, Se, Te), has attracted much attention[2–5] since it offers a versatile range of relevant physical properties. The A_2BX_4 group currently consists of ∼800 documented members[6] with possible applications as transparent conductors (Cd_2SnO_4 and In_2MgO_4), thin film transistor materials (Zn_2SnO_4), lithium-ion battery materials (Mn_2LiO_4 and Co_2LiO_4), and thermoelectrics (Cr_2CuSe_4 and Cr_2FeS_4). Interestingly, however, reviewing the two standard inorganic chemistry databases: (1) the inorganic chemistry structural database—ICSD[7,8]—that records ∼130 000 inorganic substances with completely identified crystal structures and (2) the *powder diffraction file*—ICDD PDF[9]—that lists ∼300 000 x-ray diffraction data sets, we find that an additional ∼3000 A_2BX_4 members can be written down formally but are not reported. One wonders then how many unreported compounds are intrinsically (thermodynamically) unstable, and how many *should* exist but have yet to be explored, with potentially game-changing material functionality.

Along with high-throughput electronic band structure calculations for ICSD-existing materials,[10] knowledge-driven high-throughput computational techniques based on data mining[11,12] have been used to predict ∼200 new oxide ternary compounds.[13] On the other hand, quantum calculations of unknown materials without assessing their thermodynamic stability[14–16] continue to suggest promising physical properties in potentially unstable materials. One might suspect that certain metastable structures are kinetically sufficiently protected against thermodynamic instabilities to have usefully long lifetimes including nearly all semiconductor superlattices grown from the gas phase[17–19] or nitrogen dissolved in ZnO from a high-energy nitrous oxide source,[20] all corresponding to thermodynamically positive formation enthalpies. However, it is possible that many hypothetically conceived 3D inorganic structures might, in fact, be readily decomposable into their various constituents. Indeed, quantum predictions of interesting physical properties in hypothetical 3D inorganic materials and structures without assessing their thermodynamic stability[14–16] might correspond to structures that are insufficiently protected by kinetic barriers, preventing perhaps at the outset even their synthesis.

Here, we focus on just a subset of the A_2BX_4 compounds: those with A and B atoms being either main group elements or only one of them being a $3d$ transition metal. Specifically, two groups of such missing A_2BX_4 materials for each $X = O$,

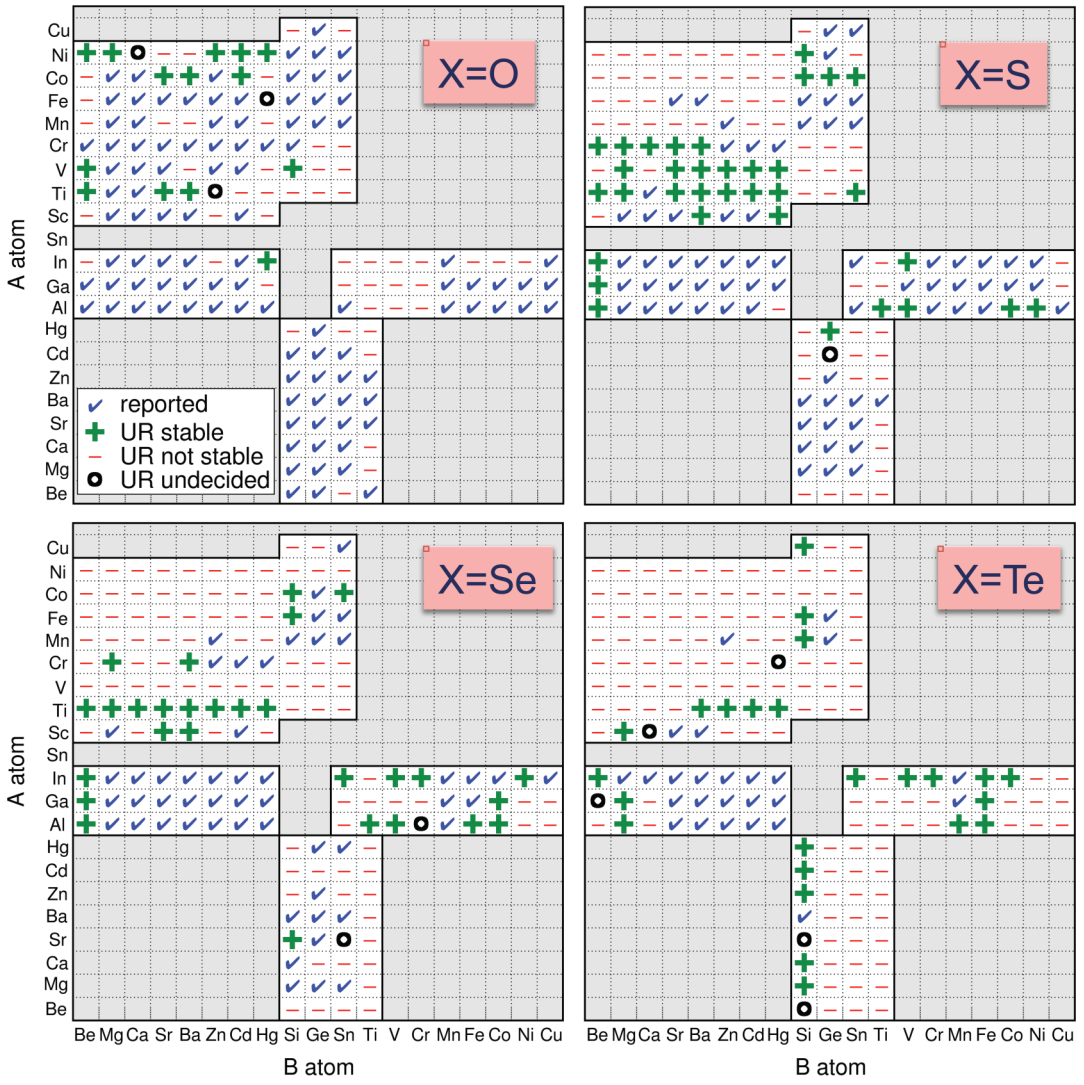

FIG. 1. (Color online) A_2BX_4 (X = O, S, Se, Te) compounds in this study. The compounds labeled by plus, minus, and circle signs are unreported (UR) in ICSD and ICDD PDF.

S, Se, and Te can be constructed. In Fig. 1 we indicate those compounds that have been reported in the literature with a check mark, whereas all entries in Fig. 1 that are listed with a symbol (see legend) that includes "UR" are currently unreported. The groups considered are: (1) III_2-II-VI_4, III = Al, Ga, In, II = Be, Mg, Ca, Sr, Ba, Zn, Cd, Hg, Sn, 3*d* elements except Sc; or III = 3*d* elements except Cu, II = Be, Mg, Ca, Sr, Ba, Zn, Cd, Hg; (2) II_2-IV-VI_4, II = Be, Mg, Ca, Sr, Ba, Zn, Cd, Hg, IV = Si, Ge, Sn, Ti; or II = 3*d* elements except Sc, IV = Si, Ge, Sn. These two groups contain 684 nominal possibilities of which 255 are reported, whereas 429 compounds are not reported neither in the ICSD nor in ICDD PDF. Using first-principles calculations of the energy of various A_2BX_4 structures as well as different combinations of binary and other competing phases (see Fig. 2), we find that out of 429 missing compounds 318 are unstable with respect to competing phases and 11 are too close to call. On the other hand, we find 100 A_2BX_4 compounds that are thermodynamically stable including 14 oxides, 34 sulfides, 28 selenides, and 24 tellurides. We determine the crystal structures in which they are stable both with respect to decomposition into pure elements (negative formation enthalpy) and to decomposition into combinations of pure elements and other

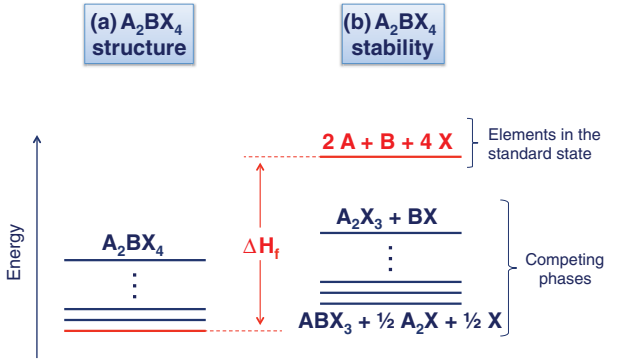

FIG. 2. (Color online) Schematic illustration of testing the thermodynamic stability of a hypothetical A_2BX_4 compound by comparing total energies.

binary and/or ternary compounds. The list of yet undiscovered 100 metal chalcogenides is interesting because (i) they display fascinating chemical trends from oxides to tellurides, (ii) some of them contain elements in their rare oxidation states (e.g., Ti^{3+}) or uncommon coordinations, and (iii) dozens of them are not hard to synthesize in terms of growth condition, as estimated from first-principles calculations.

II. APPROACH FOR DETECTING OVERLOOKED A_2BX_4 COMPOUNDS

Figure 2 illustrates some of the *burden of proof* required to predict the existence of multinary compounds. One faces two main problems. Firstly, there is a question of the lowest-energy crystal structure of an unknown ternary compound. This is a complex problem as there are, in principle, infinitely many possibilities. Second is the question of the stability of a given compound with respect to decomposition into its competing phases, such as either pure A, B, and X elements, or combinations of the pure elements with other binary and/or ternary compounds within the same A-B-X chemical system. In this section we describe our approach to solving these two problems.

A. Determination of the structure type of a specific ternary A_2BX_4 compound

The problem of the lowest-energy crystal structure of a multinary compound can be solved successfully by applying the global space group optimization (GSGO) method.[21] The input of the GSGO method consists of random lattice vectors and random Wyckoff atomic positions, so the structure is unbiased. It then uses a real-space genetic-algorithm selection of structures, involving structure mating and mutation. The approach uses a sequence of *ab initio* density functional evaluation of total energies of locally relaxed trial structures so as to seek the lowest-energy structure. Such GSGO typically requires significant computational resources to solve the low-energy structure problem for a single set of A, B, and X elements. It is not tractable within high-throughput approaches that aim at predicting a large number of missing/potentially overlooked compounds.

Alternatively, one can construct a set of likely candidate crystal structure types for A_2BX_4 and compute their total energies subject to local relaxation, then select the lowest-energy structure from this list. The list of candidate structure types is created from those which are known from existing A_2BX_4 compounds. It has been shown in Ref. 6 that ~800 reported A_2BX_4 compounds crystallize in 32 different structure types. Out of 32 we exclude four since each of them represents only one reported A_2BX_4 compound containing either Li or H. We enrich the set of structure types by recognizing an important structural feature of ternary materials, the possibility that the A and B atoms exchange their lattice sites. For example, spinels are known to exist in the normal spinel structure, where the A atoms are octahedrally coordinated and the B atoms are tetrahedrally coordinated (as in Al_2MgO_4), and in the inverse spinel structure which is equivalent to a 50%-50% alloy of A and B atoms over the octahedral sites (such as Mg_2TiO_4[22]). By reviewing the ICSD database, it can be found that out of the 28 relevant structure types, 12 can exist in this "inverted" modification. Under the assumption that the ground states of these 12 inverted structures can be constructed in the same way as in spinel oxides, that is, by making the inverse configurations on a single primitive cell,[23] we obtain a set of 40 candidate A_2BX_4 structure types, listed in Table I.

For each unreported $\{A,B,X\}$ combination, we compute the total energies of all 40 structure types by relaxing all external (cell shape) and all internal (atomic positions) degrees of freedom. The electronic degrees of freedom are described within the density functional theory in the GGA + U approximation. In all our calculations, spin degrees of freedom have been included explicitly and the total magnetization is also relaxed to the ground state.[24–27] Computing total energies of different magnetic configurations for 40 structure types for each of the examined 429 A_2BX_4 combinations amounts to ~70 000 independent DFT calculations. This includes different stages of the relaxation procedure (needed because of the cell-shape relaxation) and different starting magnetic configurations. This number of calculations requires automatization of the computational process that is applied in this paper. Finally, for any given A_2BX_4, after calculating total energies of all 40 structure types in different magnetic configurations, it is possible to sort out the lowest-energy structure.

B. Calculating competing phases

a. Corrected DFT formation enthalpies of compounds. Having established the lowest-energy structure type of A_2BX_4 [red/gray line in Fig. 2(a)], the next task is to determine if this ternary compound is stable with respect to a decomposition into its competing phases [see Fig. 2(b)]. To do this, one ultimately needs to obtain accurate formation energies of all decomposition reactions involving the A_2BX_4 under consideration. This requires knowing the formation enthalpies ΔH_f (i.e., the energy needed to form a compound out of its elemental constituents in their standard forms) for both the A_2BX_4 and its competing phases with relevant accuracy. However, standard approximations to DFT, namely, the LDA and GGA, are known[28,29] to do poorly at predicting the ΔH_f values for the semiconductor compounds. In case of transition metal (TM) compounds, which can occur in different oxidation states of the TM element, there exists an additional source of uncertainty: due to the residual self-interaction error, standard DFT tends to favor energetically the compounds with higher TM oxidation states (lower d occupancies), which can lead to unrealistic predictions about the stability or instability of compounds with certain compositions.[28,30,31] For instance, NiO is wrongly predicted to be unstable with respect to Ni_2O_3 (i.e., the reaction $3NiO \rightleftarrows Ni_2O_3 + Ni$ goes forward) at low temperature and low pressure. However, DFT + U is an effective remedy for this error.[32] In the case of direct ΔH_f calculations, however, DFT + U suffers from the problem that numerical values for U that correct the relative stability of different oxidation states in the compounds lead to serious errors in the total energies of pure metallic elemental phases. These errors do not cancel out when computing ΔH_f.

Formation enthalpies correspond to total energy difference between a compound AB and the standard elemental phases

TABLE I. List of 40 candidate crystal structure types of A_2BX_4 compounds. The labels are taken from Ref. 51 except labels S1–S3 that indicate the Y_2MnS_4-type, Yb_3S_4-type and Sr_2PbO_4-type structures, respectively. Structure types that exist in the inverted modification (see text) are indicated with the capital I letter.

Label	Prototype compound	Space group no.	Pearson's symbol/mineral name	Number of occurence
b5/b5I	Al_2MgO_4	Fd-3m(227)	cF56/Spinel	255
d9	Th_3P_4	I-43d(220)	cI28	87
b9/b9I	Fe_2CaO_4	$Pnma$(62)	oP28	78
b11	K_2SO_4	$Pnma$(62)	oP28	69
d3/d3I	Cr_3S_4	$C2/m$(12)	mS14	57
b10/b10I	Al_2BeO_4	$Pnma$(62)	oP28/Olivine	48
b1/b1I	K_2MgF_4	$I4/mmm$(139)	tI14	41
b6	Mn_3O_4	$I4_1/amd$(141)	tI28/Hausmanite	27
b4/b4I	Ag_2HgI_4	P-42m(111)	tP7/	24
	Al_2CdS_4	I-4(82)	tI14/Thiogallate	
b33	Li_2WO_4	R-3	hR42/Phenakite	14
S1/S1I	Y_2MnS_4	$Cmcm$(63)	oS28	14
S2/S2I	Yb_3S_4	$Pnma$(62)	oP28	13
d1/d1I	Pb_3O_4	$P4_2/mbc$(135)	tP28/Minium	9
b21	Al_2BaO_4	$P6_322$(182)	hP56	7
S3/S3I	Sr_2PbO_4	$Pbam$(55)	oP14	6
b18	Na_2SO_4	$Fddd$(70)	oF56/Thenardite	4
b2/b2I	K_2PtCl_4	$P4/mmm$(123)	tP7	3
b7	Cr_2CuO_4	I-42d(122)	tI28/distorted Spinel	2
b20	Pb_2SO_4	$P6_3$(173)	hP14	2
b8	Ti_2CaO_4	$Cmcm$(63)	oS28	1
b12	Ba_2TiO_4	$P2_1/c$(14)	mP28	1
b19	Na_2CrO_4	$Cmcm$(63)	oS28	1
b34	Bi_2PbS_4	$Pnma$(62)	oP28/Galenobismuthite	1
b35	Sb_2FeS_4	$Pnma$(62)	oP28/Berthierite	1
b36	As_2PbS_4	$P2_1/c$(14)	mP28/Scleroclase	1
b37	Sb_2SnTe_4	R-3m(166)	hR7	1
b38	In_2ZnS_4	$R3m$(160)	hR7	1

(not free atoms) $A + B$. In compounds where AB, A, and B are all metallic solid, the calculation of ΔH_f can benefit from cancellation of errors associated with similarly imperfect description of bonding in AB and its constituent solids A and B. However, when some of elemental constituents of AB are metals and other nonmetals—as is the case for metal chalcogenides or metal pnictides—we may not benefit from systematic cancellation of errors in evaluating the energies of AB, A and B (e.g., when B is the O_2 molecule and A is a transition metal in the solid phase). The ideal approach might then be to move to an electronic structure method that is of equivalent accuracy for the bonding types underlying AB, A and B such as perfect quantum Monte Carlo (QMC).[33] Here, we employ instead a simple method that can be applied consistently to AB, A and B: a computationally inexpensive theoretical approach based on GGA + U calculations with "fitted elemental-phase reference energies" (FERE).[29,31] A set of 252 measured enthalpies of formation ΔH_f values for binary compounds (pnictides, chalcogenides, and halides) is used to fit to FERE energies for 50 elements. This reproduces the enthalpies of formation to within a rather low error.[31] The predictive power of the FERE approach is demonstrated on a set of 55 ternary compounds that were not part of the fitting set.[31] This calculation is done using GGA + U with a fixed U ($J = 0$). This is not meant to fix the band structure, but the formation enthalpy. We find that our approach using $U = 3$ ($J = 0$) eV for 3d transition metals (except 5 eV for Cu) reproduces the experimentally measured formation enthalpies with a root mean square error of 0.07 eV/atom. We do not apply these U values to metals but use fitted elemental reference energies for them because DFT + U leads to serious errors in the total energies of pure metallic elemental phases. We have selected here the approach of using the simplest approximation that works—as long as the resulting FERE-corrected formation enthalpies of ∼250 binary compounds still agree with calorimetry experiment (see Ref. 31). We see no reason to introduce variable U values at this point, as the simplest choice is consistent with all data.

b. Identification of the chemical potential range. Accurate ΔH_f formation enthalpies provide simple ways to analyze the stability of a given compound by computing the heats of all decomposition reactions involving pure elements in combination with other competing phases within the same chemical system.[34]

c. Ground-state structures: canonical representation. The ground-state structure of a compound with a given composition (e.g., NiO) can be found by directly comparing the total energies of possible crystal structures. For various compositions (e.g., Ni_xO_{1-x} system), the formation enthalpies provide a simple way to represent the ground-state line (the convex

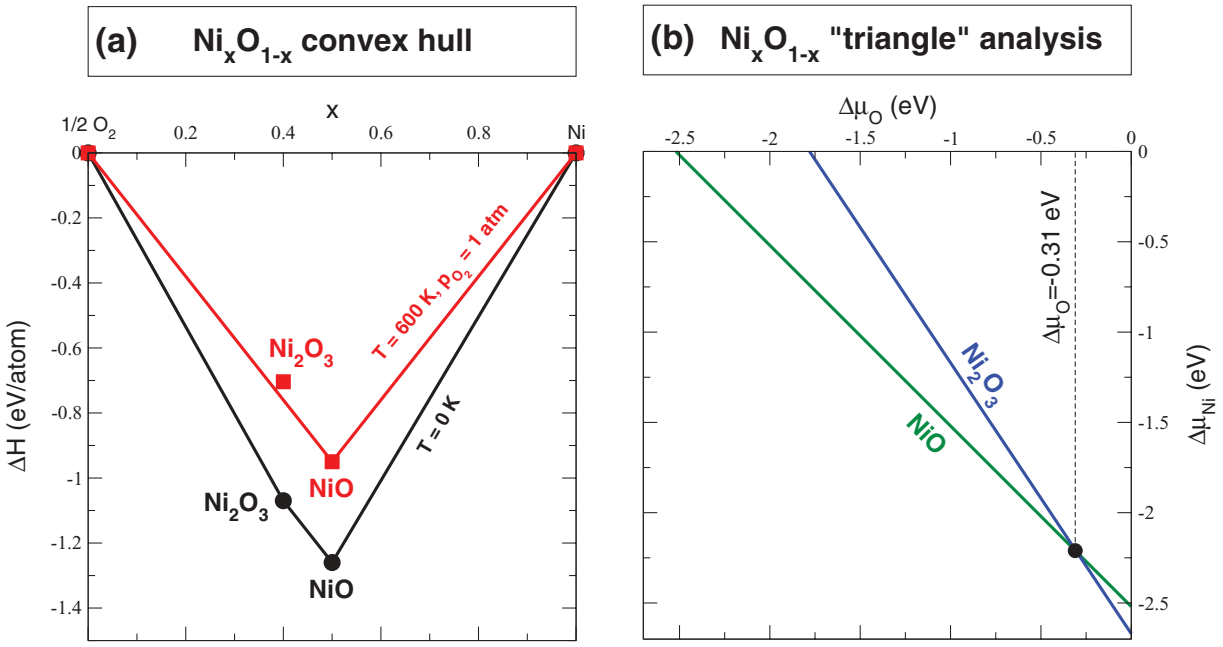

FIG. 3. (Color online) (a) Ground-state lines of Ni_xO_{1-x} system for $T = 0$ (black line) and 600 K (red/gray line). (b) Chemical potential diagram of Ni_xO_{1-x} system.

hull) as shown in Fig. 3(a) for the Ni_xO_{1-x} system. At each fixed composition (canonical ensemble), the compound on the ground-state line, e.g., NiO with 50 : 50 composition, has lower energy than any linear combination of other compounds in this system that sum up to the examined composition (e.g., NiO). Therefore the compounds on ground-state line are all stable with respect to disproportionation into their competing phases. The convex hull has been extensively used before.[35–39]

d. Chemical potential diagram: grand canonical representation. In this paper, we use an alternative, to some extent more general approach.[40,41] The formulation[40,41] is in the grand-canonical ensemble and is phrased in terms of the chemical potentials of the constituent atoms as given by a set of equality and inequalities [e.g., Eqs. (1)–(3) for NiO]:

$$\Delta\mu_{\mathrm{Ni}} + \Delta\mu_{\mathrm{O}} = \Delta H_f(\mathrm{NiO}), \tag{1}$$

$$\Delta\mu_I \leqslant 0, (I = \mathrm{Ni,O}), \tag{2}$$

$$2\,\Delta\mu_{\mathrm{Ni}} + 3\,\Delta\mu_{\mathrm{O}} \leqslant \Delta H_f(\mathrm{Ni_2O_3}), \tag{3}$$

with $\Delta\mu_I = \mu_I - \mu_I^0$ ($I = \mathrm{Ni,O}$) the deviation of the actual chemical potentials from the their μ_I^0 values.[29,31] Equation (1) defines the thermodynamic equilibrium and sets the allowed ranges [green/light gray line in Fig. 3(b)] for $\Delta\mu$'s (together with the condition $\Delta\mu_I \leqslant 0$). The inequality (3) defines the condition [i.e., graphically in the area below the blue/dark gray line in Fig. 3(b)] under which it is more favorable to form NiO over the competing phase Ni_2O_3. This way of representing the stability of compounds is common in the study of defects in semiconductors[41,42] and is exactly equivalent to the linear programming approach described in Ref. 39. The idea is to find the ranges of chemical potentials within which it is energetically most favorable that a given compound forms instead of any combination of its competing phases. This representation provides directly the information on the stability of different compounds when coupled to the reservoirs of particles (e.g., oxygen gas) the state of which is given with a set of macroscopic parameters such as pressure and temperature. For example, it is Ni_2O_3 that is more favorable to form for $\Delta\mu_{\mathrm{O}} > -0.31$ eV, whereas at the oxygen chemical potentials lower than this value, NiO form is more favorable. This grand canonical representation has two main advantages: (i) it covers at the same time various external conditions and (ii) it also describes what happens when a system is coupled to a reservoir of particles, which is often a case in real experiments.

For a given A_2BX_4 compound, in order to be thermodynamically stable, similar to Eqs. (1)–(3) the following set of equality and inequalities needs to be satisfied:

$$2\,\Delta\mu_A + \Delta\mu_B + 4\,\Delta\mu_X = \Delta H_f(A_2BX_4), \tag{4}$$

$$\Delta\mu_I \leqslant 0, (I = A, B, X), \tag{5}$$

$$n^{(i)}\,\Delta\mu_A + m^{(i)}\,\Delta\mu_B + q^{(i)}\,\Delta\mu_X \leqslant \Delta H_f(A_{n^{(i)}}B_{m^{(i)}}X_{q^{(i)}}), \quad i = 1, \ldots, Z, \tag{6}$$

with Z the total number of binary and ternary competing phases with chemical formulae $A_{n^{(i)}}B_{m^{(i)}}X_{q^{(i)}}$ and formation enthalpies $\Delta H_f(A_{n^{(i)}}B_{m^{(i)}}X_{q^{(i)}})$. Equation (4) defines a triangle in the three-dimensional $(\Delta\mu_A, \Delta\mu_B, \Delta\mu_X)$ space, instead of a line in binary case (e.g., green/light gray line in Fig. 3). Inside a certain region of the triangle, if, for example, one of the inequalities (6) is violated, then within this region it is energetically more favorable for the corresponding competing phase to form instead of the A_2BX_4. If there is a violation of at least one of the inequalities (6) at any point inside the triangle

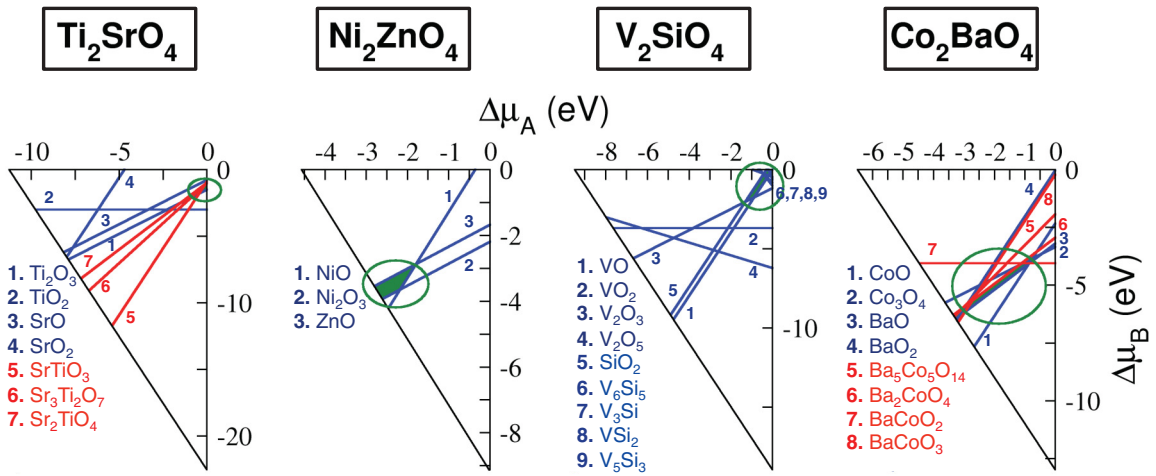

FIG. 4. (Color online) Thermodynamic stability analysis of Ti_2SrO_4, Ni_2ZnO_4, V_2SiO_4, and Co_2BaO_4, which have typical stability $\Delta\mu_I$ regions shown as green/light gray areas. For clarity, we project the 3D chemical potential diagram onto the 2D plane of $\Delta\mu_A$ and $\Delta\mu_B$. The blue/dark gray (red/gray) line is the cutting edge of the competing binary (ternary) phase, which cuts off a part of the triangle on one side of the line. For the chemical potentials ($\Delta\mu_I$'s) inside the rest green/light gray area, the A_2BX_4 compound is energetically favorable. If $\Delta\mu_I$'s go outside of the green/light gray area (e.g., towards the bottom right corner of Ni-rich, O-rich and Zn-poor condition in Ni_2ZnO_4 case), certain competing phases (e.g., NiO and Ni_2O_3) become energetically more favorable than the A_2BX_4 compound.

then the A_2BX_4 compound is predicted unstable under the thermodynamic equilibrium conditions, otherwise the A_2BX_4 is thermodynamically stable (as illustrated in Fig. 4).[43] Since the $\Delta\mu$'s describe the state of the source of pure elements, the region of the triangle within which the examined A_2BX_4 forms can be directly translated to the needed growth conditions. In the case of oxides, the range of $\Delta\mu_O$ for which the A_2BX_4 forms can be translated into ranges of oxygen partial pressure and temperature needed for growth.

C. Summary of the algorithm for predicting A_2BX_4 compounds

This section summarizes the methodology for detecting overlooked A_2BX_4 compounds. The algorithm is schematically presented in Fig. 5. After choosing the A-B-X chemical system for which there are no reported A_2BX_4 compounds in either the ICSD or the ICDD PDF databases, we perform a set of high-throughput *ab initio* calculations to sort out the ground-state structure of A_2BX_4 and to compute its formation enthalpy. For these purposes, we need the set of candidate structure types and the database of fitted μ^0 values as explained in Sec. II, respectively. Next comes the triangle stability analysis. In order to do this, we need a list of all binary and ternary competing phases together with their ΔH_f values. The ΔH_f values are computed on the reported ICSD structures utilizing the same set of fitted μ_0 values.[31] If the stability analysis results in a finite ranges for $(\Delta\mu_A, \Delta\mu_B, \Delta\mu_X)$, we arrive at the prediction for the existence of a new A_2BX_4 compound.

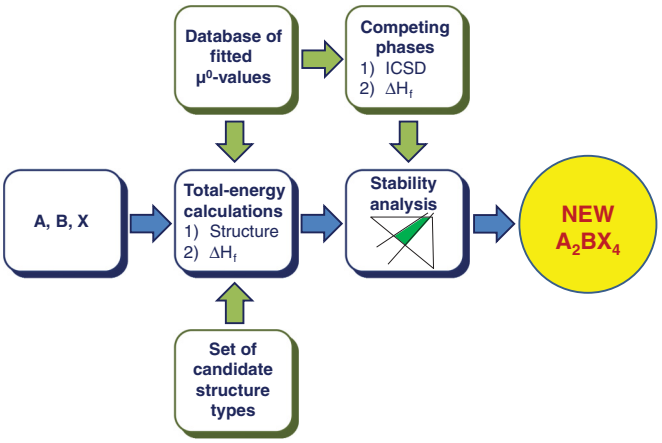

FIG. 5. (Color online) Theoretical procedure for predicting stable A_2BX_4 compounds.

We test the algorithm on seven known compounds: Mn_2SiO_4, Sr_2TiO_4, Al_2ZnS_4, Ba_2TiS_4, Ca_2SiS_4, Sc_2MgSe_4, and In_2MgTe_4. We found them to be thermodynamically stable and found their lowest-energy structures to be b10, b1, b5, b11, b10, b5, b4, in agreement with experiments.[7,8] The limitations of our approach are (i) the accuracy of the prediction on compound stability and growth condition is limited by the tolerance of ΔH_f calculation,[31,43] (ii) we do not consider the temperature effect on solid compounds, (iii) some known competing phases are not included, e.g, noninteger compounds and metal gas, which are not tractable within high-throughput approaches at this moment, (iv) we do not consider the unknown competing phases[44] which may be discovered and characterized by experiment in future, (v) the kenetic barriers in growth conditions are not considered.

III. RESULTS AND DICUSSION

A. Unreported but predicted stable A_2BX_4

Having constructed the high-throughput algorithm, we apply it to investigate the 429 missing A_2BX_4 compounds

TABLE II. List of unreported A_2BX_4 oxides predicted to be stable (14 compounds in total). Predicted structure, the ΔH_f value (in eV/atom), $\Delta\mu_O^{\min}$ and $\Delta\mu_O^{\max}$ (in eV) are presented. Ti_2ZnO_4 (b5), Fe_2HgO_4[†] (b6), and Ni_2CaO_4 (b9) are too close to call.

A_2BX_4	Structure type	ΔH_f	$\Delta\mu_O^{\min}/\Delta\mu_O^{\max}$	A_2BX_4	Structure type	ΔH_f	$\Delta\mu_O^{\min}/\Delta\mu_O^{\max}$
Co_2BaO_4	b21	−1.86	−1.81/−0.17	Ni_2MgO_4[†]	b5	−1.69	−0.55/0.0
Co_2CdO_4[a]	b5	−1.33	−0.28/0.0	Ni_2ZnO_4[†]	b6	−1.32	−0.68/0.0
Co_2SrO_4	b10I	−1.89	−1.30/0.0	Ti_2BaO_4	b10I	−3.15	−5.26/−5.13
In_2HgO_4	b5	−1.49	−3.78/0.0	Ti_2BeO_4	b10	−3.12	−5.25/−3.67
Ni_2BeO_4	b10	−1.64	−0.36/0.0	Ti_2SrO_4	b9	−3.20	−5.34/−4.97
Ni_2CdO_4[†]	b6	−1.16	−0.49/0.0	V_2BeO_4	b10	−2.78	−3.88/−1.88
Ni_2HgO_4	b10I	−0.91	−0.42/0.0	V_2SiO_4[†]	b6	−2.71	−4.46/−3.56

[a]New oxides also predicted by Hautier *et al.*[13]

(shown as plus, minus, or circle signs[43] in Fig. 1). We find 100 stable A_2BX_4 including 14 oxides, 34 sulfides, 28 selenides, and 24 tellurides, which are diagrammatically shown as green/light gray plus signs in Fig. 1. Together with the reported compounds, we now have 119 oxides, 107 sulfides, 80 selenides, 49 tellurides (blue/dark gray check marks and green/light gray plus signs in Fig. 1). By doing systematic triangle analysis on the lowest-energy structure of the missing A_2BX_4 compounds, we find a large amount of them missing for a good reason (shown as red/gray minus signs in Fig. 1), i.e., they are thermodynamically unstable or metastable with respect to decomposition into competing phases. Especially, ∼2/3 of tellurides and half of selenides we considered are found to be thermodynamically unstable.

Among the 100 stable compounds missing in ICSD and ICDD PDF, V_2CdS_4[45] was synthesized and well characterized to be in b5 (cubic spinel) structure, and we find that its lowest-energy structure is actually a slightly distorted spinel structure. Furthermore, Al_2MnTe_4,[46] V_2SrS_4, Cr_2SrS_4, Cr_2BaS_4 Cr_2BaSe_4,[47] Co_2SnS_4, and Ti_2SnS_4[48] were synthesized but not fully characterized.

The lowest-energy structures of the predicted A_2BX_4 compounds are identified by the high-throughput approach, as shown in Tables II–V. We are aware of the fact that certain compounds are dynamically unstable in certain crystal structures. In those cases, there exist lower-energy dynamically stable structures, and some of them are reported in experiments (e.g., see Table I), the others are unknown and hard to guess that can be searched by the GSGO method. We use the GSGO[49] approach as a "sanity check" to verify our results from high-throughput approach on two out of the 100 A_2BX_4 compounds predicted here due to the limitation of computation source. The lowest-energy structures found by GSGO for the two compounds Ga_2MgSe_4 and In_2BeTe_4 are both the thiogallate structure, in agreement with the results from the high-throughput approach. We are aware of the fact that metastable materials in higher-energy structures can sometimes be made, and could exist for long times. The

TABLE III. List of unreported A_2BX_4 sulfides predicted to be stable (34 compounds in total). Predicted structure, the ΔH_f value (in eV/atom), $\Delta\mu_S^{\min}$ and $\Delta\mu_S^{\max}$ (in eV) are presented.

A_2BX_4	Structure type	ΔH_f	$\Delta\mu_S^{\min}/\Delta\mu_S^{\max}$	A_2BX_4	Structure type	ΔH_f	$\Delta\mu_S^{\min}/\Delta\mu_S^{\max}$
Al_2BeS_4	b4I	−1.39	−2.38/0.0	Ni_2SiS_4	b10	−0.69	−0.52/−0.35
Al_2CoS_4	b6	−1.22	−1.44/0.0	Sc_2BaS_4	b34	−2.31	−3.06/−0.03
Al_2NiS_4	b5I	−1.17	−0.56/−0.34	Sc_2HgS_4	b6	−1.67	−0.66/0.0
Al_2TiS_4	b10I	−1.47	−2.47/−1.46	Ti_2BaS_4	b36	−1.84	−2.08/−0.81
Al_2VS_4	b10I	−1.44	−2.43/−0.07	Ti_2BeS_4	b7	−1.48	−1.32/−0.91
Co_2GeS_4	b4I	−0.56	−0.95/−0.40	Ti_2CdS_4	b7	−1.39	−1.78/−0.72
Co_2SiS_4	b4I	−0.74	−1.06/−0.21	Ti_2HgS_4	b37	−1.26	−1.11/−0.41
Co_2SnS_4	b4I	−0.57	−0.84/−0.24	Ti_2MgS_4	b7	−1.64	−1.83/−0.72
Cr_2BaS_4[a]	S2I	−1.41	−1.10/−0.12	Ti_2SnS_4	b36	−1.27	−1.03/−1.00
Cr_2BeS_4	b10	−1.08	−0.76/0.0	Ti_2SrS_4	b34	−1.85	−1.93/−0.68
Cr_2CaS_4	b9	−1.40	−0.82/0.0	Ti_2ZnS_4	b7	−1.46	−2.08/−0.65
Cr_2MgS_4	b6	−1.25	−1.37/0.0	V_2BaS_4	S2I	−1.54	−0.33/−0.17
Cr_2SrS_4[a]	b34	−1.42	−0.90/0.0	V_2CdS_4[a]	b7	−1.10	−0.39/−0.08
Ga_2BeS_4	b4I	−1.10	−0.92/0.0	V_2HgS_4	b7	−0.94	−0.43/−0.07
Hg_2GeS_4	b4I	−0.41	−0.57/0.0	V_2MgS_4	b7	−1.36	−0.35/−0.08
In_2BeS_4	b4I	−0.94	−0.90/0.0	V_2SrS_4[a]	b34	−1.56	−0.36/−0.08
In_2VS_4	b5I	−0.99	−1.09/−0.03	V_2ZnS_4	b7	−1.17	−0.45/−0.07

[a]These compounds are neither in ICSD nor in ICDD PDF but can be found in Refs. 45 and 47.

TABLE IV. List of unreported A_2BX_4 selenides predicted to be stable (28 compounds in total). Predicted structure, the ΔH_f value (in eV/atom), $\Delta\mu_{\mathrm{Se}}^{\mathrm{min}}$, and $\Delta\mu_{\mathrm{Se}}^{\mathrm{max}}$ (in eV) are presented.

A_2BX_4	Structure type	ΔH_f	$\Delta\mu_{\mathrm{Se}}^{\mathrm{min}}/\Delta\mu_{\mathrm{Se}}^{\mathrm{max}}$	A_2BX_4	Structure	ΔH_f	$\Delta\mu_{\mathrm{Se}}^{\mathrm{min}}/\Delta\mu_{\mathrm{Se}}^{\mathrm{max}}$
Al_2BeSe_4	b4I	−1.06	−1.84/0.0	In_2NiSe_4	b5I	−0.54	−0.33/0.0
Al_2CoSe_4	b4	−0.91	−0.92/0.0	In_2SnSe_4	b10I	−0.60	−0.36/0.0
Al_2FeSe_4	b4I	−0.94	−1.07/0.0	In_2VSe_4	b5I	−0.78	−0.53/0.0
Al_2TiSe_4	b10I	−1.14	−1.88/−1.24	Sc_2BaSe_4	b9	−2.04	−2.86/0.0
Al_2VSe_4	b10I	−1.11	−1.87/0.0	Sc_2SrSe_4	b9	−2.02	−2.75/0.0
Co_2SiSe_4	b4I	−0.45	−0.56/−0.08	Sr_2SiSe_4	b10	−1.55	−0.85/0.0
Co_2SnSe_4	b4	−0.36	−0.43/−0.14	Ti_2BaSe_4	b34	−1.56	−1.45/−0.54
Cr_2BaSe_4[a]	S2I	−1.17	−0.35/0.0	Ti_2BeSe_4	b7	−1.15	−0.92/−0.70
Cr_2MgSe_4	b6	−0.96	−0.76/0.0	Ti_2CaSe_4	d3	−1.50	−0.89/−0.72
Fe_2SiSe_4	b10	−0.49	−0.78/0.0	Ti_2CdSe_4	b7	−1.12	−1.25/−0.60
Ga_2BeSe_4	b4I	−0.85	−0.55/0.0	Ti_2HgSe_4	b37	−1.00	−0.87/−0.40
Ga_2CoSe_4	b4	−0.71	−0.72/0.0	Ti_2MgSe_4	b6	−1.33	−1.39/−0.56
In_2BeSe_4	b4I	−0.74	−0.52/0.0	Ti_2SrSe_4	b9	−1.55	−1.13/−0.66
In_2CrSe_4	b5I	−0.68	−0.31/0.0	Ti_2ZnSe_4	b7	−1.16	−1.46/−0.54

[a]This compound is neither in ICSD nor in ICDD PDF but can be found in Ref. 47.

higher-energy structures of the 100 stable A_2BX_4 compounds are given in Appendix A.

Some of the predicted compounds contain elements in uncommon coordinations, e.g., (i) Mg surrounded by O_4 tetrahedron (instead of normal O_6 octahedron) in Ni_2MgO_4, (ii) Cd surrounded by O_4 tetrahedron (instead of normal O_6 octahedron) in Ni_2CdO_4 and Co_2CdO_4, (iii) Ca surrounded by S_8 polyhedron (instead of normal S_6 octahedron) in Cr_2CaS_4, and (iv) Sr surrounded by Se_8 polyhedron (instead of normal Se_6 octahedron) in Sc_2SrSe_4 and Ti_2SrSe_4. Variation of coordination environment affects the atomic bondings, so also affects the electronic structure of the compound.

A number of predicted A_2BX_4 compounds contain elements in their rare oxidation states (ROS), e.g., (i) Ti^{3+} in Ti_2BaO_4, Ti_2BaS_4, Ti_2CdS_4, Ti_2CdTe_4, etc., (ii) Ti^{2+} in Al_2TiS_4 and Al_2TiSe_4, (iii) V^{2+} in Al_2VS_4, In_2VS_4, Al_2VSe_4, In_2VSe_4, and In_2VTe_4, and (iv) Cr^{2+} in In_2CrSe_4 and In_2CrTe_4. Usually, ternary compounds with elements in their normal oxidation states (NOS) (e.g., $CaTiO_3$) are expected to be more likely than those containing elements in ROS (e.g., Ti_2CaO_4). However, we find that Ti_2AX_4 (A = Be, Mg, Ca, Sr, Ba, Zn, Cd, Hg, X = S, Se, Te) compounds with Ti in its ROS Ti^{3+} are much more likely (20 out of 24 are stable) than A_2TiX_4 compounds that have Ti in its NOS Ti^{4+} (1 out of 24 are stable). The unstable A_2TiX_4 compounds are energy unfavorable because the competing phases $2(AX) + TiX_2$ (e.g., 2CaSe + $TiSe_2$) without elements in ROS are comparably stable and have lower energy than A_2TiX_4, e.g., 2CaSe + $TiSe_2$ are 0.089 eV/atom lower in energy than Ca_2TiSe_4. Our results emphasize the possibility of searching new materials in the wide arena of hypothetic compounds with elements in ROS.

TABLE V. List of unreported A_2BX_4 tellurides predicted to be stable (24 compounds in total). Predicted structure, the ΔH_f value (in eV/atom), $\Delta\mu_{\mathrm{Te}}^{\mathrm{min}}$, and $\Delta\mu_{\mathrm{Te}}^{\mathrm{max}}$ (in eV) are presented.

A_2BX_4	Structure type	ΔH_f	$\Delta\mu_{\mathrm{Te}}^{\mathrm{min}}/\Delta\mu_{\mathrm{Te}}^{\mathrm{max}}$	A_2BX_4	Structure type	ΔH_f	$\Delta\mu_{\mathrm{Te}}^{\mathrm{min}}/\Delta\mu_{\mathrm{Te}}^{\mathrm{max}}$
Al_2FeTe_4	b4I	−0.52	−0.31/0.0	In_2CrTe_4	d3	−0.40	−0.06/0.0
Al_2MgTe_4	b4	−0.80	−1.13/0.0	In_2FeTe_4	b4I	−0.35	−0.35/0.0
Al_2MnTe_4[a]	b4	−0.65	−1.14/0.0	In_2SnTe_4	S2I	−0.35	−0.04/0.0
Ca_2SiTe_4	b10	−1.03	−0.05/0.0	In_2VTe_4	b5I	−0.47	−0.14/0.0
Cd_2SiTe_4	b4	−0.37	−0.16/0.0	Mg_2SiTe_4	b10	−0.66	−0.10/0.0
Cu_2SiTe_4	b4	−0.06	−0.03/0.0	Mn_2SiTe_4	b10	−0.36	−0.15/0.0
Fe_2SiTe_4	b4I	−0.11	−0.12/0.0	Sc_2MgTe_4	b5	−1.30	−1.77/−0.02
Ga_2FeTe_4	b4I	−0.42	−0.20/0.0	Ti_2BaTe_4	b34	−1.13	−0.72/−0.25
Ga_2MgTe_4	b4	−0.69	−0.10/0.0	Ti_2CdTe_4	b7	−0.72	−0.72/−0.26
Hg_2SiTe_4	b4	−0.17	−0.20/0.0	Ti_2HgTe_4	b37	−0.61	−0.41/−0.25
In_2BeTe_4	b4	−0.44	−0.33/0.0	Ti_2ZnTe_4	b5	−0.74	−0.74/−0.24
In_2CoTe_4	b4	−0.34	−0.31/0.0	Zn_2SiTe_4	b4I	−0.39	−0.13/0.0

[a]This compound is neither in ICSD nor in ICDD PDF but can be found in Ref. 46.

B. Comparison with previous work on new oxides

A high-throughput computational technique have been applied to predict 209 oxide ternary compounds,[13] using the data mining based model to suggest the composition (e.g., $A_pB_qO_r$) and structure types. This model essentially accelerates the process of predicting new compounds along with a possibility of missing specific compounds due to (i) missing compositions $A_pB_qO_r$ containing elements in their rare oxidation states and (ii) missing lowest-energy crystal structure types. To avoid missing compounds with potentially promising functionality, we consider all nominal combinations of a set of elements in a given composition (e.g., A_2BX_4), and all relevant structure types of the known compounds. By using the latter approach, we predict 14 stable A_2BO_4 oxides (three A_2BO_4 compounds are too close to call), as listed in Table II. On the other hand, Ref. 13 considered all the A and B elements we include, and found only six A_2BO_4 compounds. Five of them are confirmed by us to be stable and one is too close to call, and the lowest-energy structures agree well. However, nine stable A_2BO_4 oxides predicted by us to be stable were not reported in Ref. 13.

C. Growth condition

The merit of doing triangle analysis is that we can simultaneously determine the stable range of chemical potentials and the thermodynamic stability of the new compounds. Figure 4 display graphically the triangle analysis performed on Ti_2SrO_4, Ni_2ZnO_4, V_2SiO_4, and Co_2BaO_4. The triangles in the 3D space defined by Eqs. (4) and (5) are projected on the 2D plane of $\Delta\mu_A$ and $\Delta\mu_B$. As shown by solid line (blue/dark gray for binary and red/gray for ternary) in the projected triangle, each competing phase cuts off a part of the triangle. The remaining green/light gray area defines the $\Delta\mu_I$ regions in which the A_2BX_4 compound is energetically favorable. Based on simple relations[50] that describe $\Delta\mu_O$ depending on temperature and oxygen partial pressure (p_{O_2}) given by the ideal-gas law (as shown in Fig. 6), and the

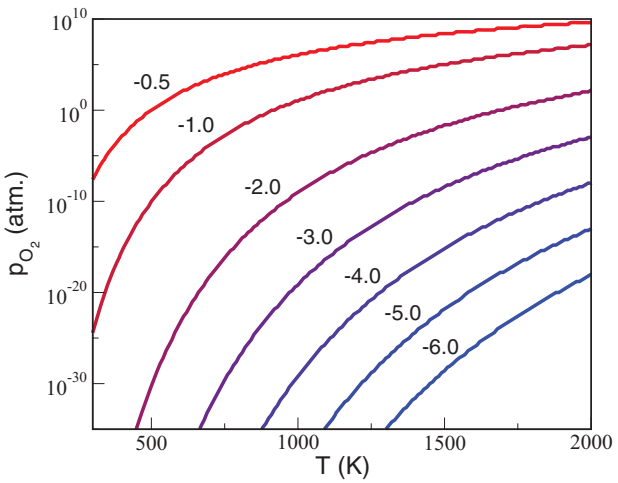

FIG. 6. (Color online) The p_{O_2} vs T diagram for a range of values of $\Delta\mu_O$.

($\Delta\mu_O^{min}, \Delta\mu_O^{max}$) stability range (as listed in Table II), one can estimate at each temperature the p_{O_2} range in which the compound can be grown in equilibrium condition. From the results in Fig. 4, Table II, and Fig. 6, we see that the growth of Ti_2SrO_4 and V_2SiO_4 need very low partial pressure at achievable temperatures, Ni_2ZnO_4 might be grown at relatively high oxidation conditions, and Co_2BaO_4 has easily achievable growth conditions while it has tiny stability area (green/light gray area) indicating a relatively small reaction enthalpy from competing phases [see Fig. 2(b)] to the A_2BX_4 compound [see Fig. 2(a)]. Our results indicate that the main reason for some of these 100 compounds to be missing from the databases are the extreme conditions needed for their synthesis. Namely, some of the predicted oxide compounds contain elements in their rare oxidation states (e.g., Ti^{3+}) needing highly reducing or highly oxidizing conditions to be stabilized, e.g., Ti_2SrO_4 as shown in Fig. 4. However, despite the possible difficulties in growing these materials, if one hopes to find unusual functionalities, compounds with elements in their atypical chemical environment is exactly the place to look for.

For A_2BX_4 sulfides, selenides, and tellurides, growth conditions are not as simple to extract from the triangle analysis as for oxides, since these elements can be solid under certain conditions, in which case the ideal gas law is not applicable. However, the calculated stability area (in eV^2) from triangle analysis [along with the corresponding stability region, e.g., ($\Delta\mu_S^{min}, \Delta\mu_S^{max}$) in Table III] is also a measure of the thermodynamic stability. As discussed above, the rare oxidation states affect the thermodynamic stability of sulfides, selenides and tellurides less than oxides. Thus the stability area calculated from triangle analysis of Ti_2SrS_4 (0.47 eV^2) is much larger than that of Ti_2SrO_4 ($\ll$0.1 eV^2). Additionally, there are dozens of compounds having large enough stability area, e.g., Ti_2BaS_4 (0.53 eV^2), Ti_2ZnS_4 (0.62 eV^2), Al_2CoS_4 (1.00 eV^2), Al_2VS_4 (0.97 eV^2), Co_2SiS_4 (0.70 eV^2), Cr_2MgS_4 (0.61 eV^2), In_2VS_4 (0.57 eV^2), Sc_2BaS_4 (2.07 eV^2), Al_2CoSe_4 (0.57 eV^2), Al_2FeSe_4 (0.83 eV^2), Al_2VSe_4 (0.60 eV^2), Fe_2SiSe_4 (0.75 eV^2), Ga_2CoSe_4 (0.51 eV^2), Sc_2BaSe_4 (1.43 eV^2), and Sc_2SrSe_4 (0.76 eV^2).

D. Emerging trends in stability and crystallography

Having completed the list of "missing A_2BX_4" (see Fig. 1), we are now in the position to observe some global trends within this group of materials. Considering all (previously known plus predicted in this paper) A_2BX_4 studied here as shown via check mark signs as well as plus signs in Fig. 1, we find that 70% of the oxides, 63% of the sulfides, 47% the selenides, and 29% of the tellurides are thermodynamically stable with respect to all possible combinations of the constituents. This rapid decline in the proportion of stable ternaries as the chalcogen atom becomes heavier reflects the larger absolute formation enthalpies of ternary oxides and sulfides relative to selenides and tellurides (see Tables II–V).

There are some patterns in the distribution of unstable compounds. (i) For A_2BO_4 oxides with A = Al, Ga, In and B = Ti, V, Cr, we find that all of the members are unstable because stabilization would have required difficulty to attain low O_2 pressures (too reducing conditions) considering the low-oxidation states of B (Ti^{2+}, V^{2+}, Cr^{2+}). In contrast to this

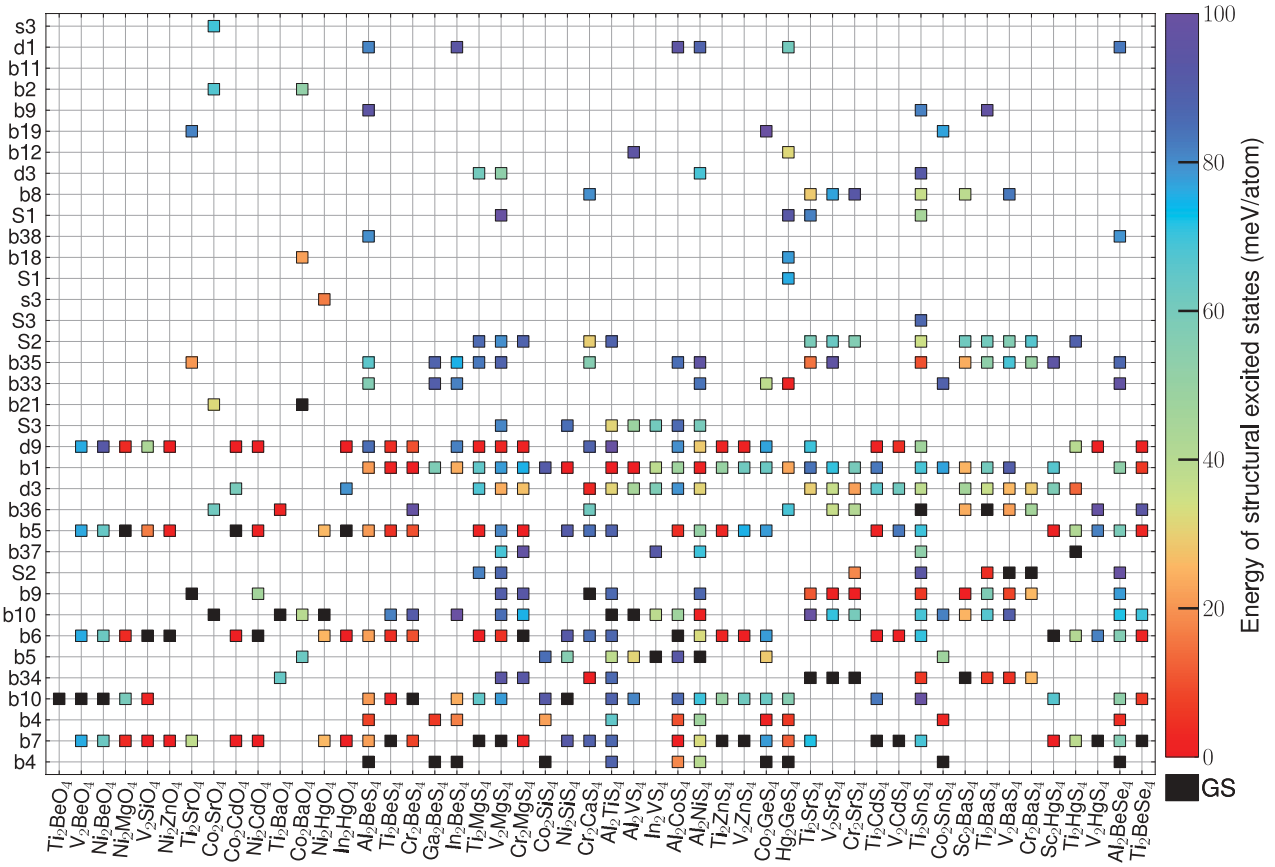

FIG. 7. (Color online) Higher-energy structures (as well as ground-state structures) of the A_2BX_4 compounds predicted here. The compound names are shown on the x axis, and the structure types (see Table I) are shown on the y axis.

trend in such oxides, their corresponding sulfides, selenides, and tellurides have some stable compounds (e.g., Al_2TiS_4, Al_2VSe_4, and In_2CrTe_4), because reducing conditions are more likely to happen in sulfides, selenides, and tellurides than oxides. (ii) For A_2BX_4 with cation $A =$ Mn, Fe, Co, Ni, $B =$ Be, Mg, Ca, Sr, Ba, Zn, Cd, Hg, and anion $X =$ O, S, Se, Te, we find that only 25% of the oxides are unstable, while 92% sulfides, 97% selenides, and 97% tellurides are unstable. The reason is that stability would require the A cations to be in the high-oxidation states (Mn^{3+}, Fe^{3+}, Co^{3+}, Ni^{3+}), which would require rather oxidizing conditions that are often not accessible in A_2BX_4 ($X =$ S, Se, Te).

In this work, we have classified all stable A_2BX_4 compounds into 40 structure types (see Table I) based on their relative DFT-calculated total energies. Previously (see Ref. 6), we have obtained such structural systematization without total energy calculation, using the concept of "orbital radii."[52] In this approach, one uses the pseudopotential free-atom s and p orbital radii (R_s and R_p) to construct a dual coordinate scheme where each A_2BX_4 compound is characterized by $R_s(A) + R_p(A)$ versus $R_s(B) + R_p(B)$ for a fixed X. The points in this plane are colored by the experimentally observed crystal structure type of each compound, and then simple boundary lines are drawn in this plane to separate areas of compounds belonging to specific structure type with as few as possible outliers (meaning a compound with a structure type different than that of the compounds in its group). The success rate is defined as a minimum number of outliers. The utility of such structure maps is in providing structural systematization of the known compounds. The orbital-radii maps have been illustrated to separate 98% successfully the structure types of the 688 known A_2BX_4 compounds and separate 96% successfully the cation distribution (normal versus inverse) of 230 known spinels.[6] Figs 9–13 in Appendix B show the boundary lines deduced in our previous work from all known A_2BX_4. In the present work, we have complemented, via total energy calculations, the previously known experimental data base of 688 A_2BX_4 by 100 additional stable A_2BX_4 not listed previously. It is interesting to enquire if their structure types could have been predicted without total energy calculations based on the previous definition of structural boundaries in orbital radii maps (see Figs. 9–13). To this end, we input the 100 additional A_2BX_4 compounds into these orbital radii maps to test their predictive ability. We found 12 outliers out of the 100 additional A_2BX_4 in the separation of structure types (see Figs. 9–12, 88% success) and two outliers in the separation of cation distribution of 31 spinels (see Fig. 13, 94% success). Interestingly, among the 12 outliers—Ni_2BeO_4, Ti_2BaO_4, Ti_2BaS_4, Ti_2SnS_4, Al_2TiSe_4, Al_2VSe_4, Ni_2HgO_4, Sc_2BaS_4, Ti_2HgS_4, Ti_2SrS_4, Ti_2CdTe_4, and Ti_2HgTe_4 in the

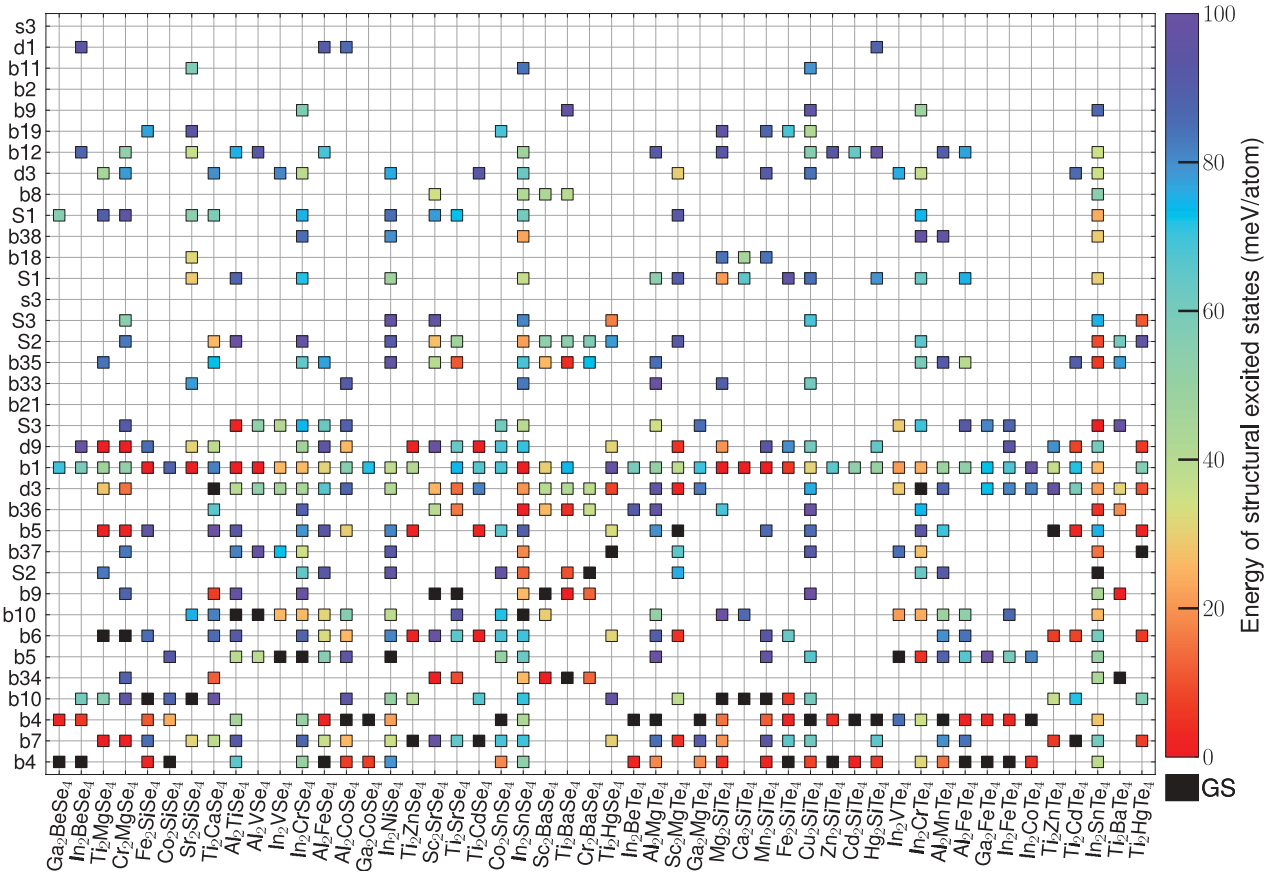

FIG. 8. (Color online) Higher-energy structures (as well as ground-state structures) of the A_2BX_4 compounds predicted here (continued).

separation of structure types, the structure type predicted by the orbital radii map corresponds in six cases (Ni_2HgO_4, Sc_2BaS_4, Ti_2HgS_4, Ti_2SrS_4, Ti_2CdTe_4, and Ti_2HgTe_4) to the second or third lowest-energy structures found in total energy calculations, which are possible to be realized in experiments.

IV. CONCLUSIONS

We developed a systematic computational approach based on first-principle Hamiltonians to predict new stable multinary compounds that have not yet been reported experimentally. This approach was successfully applied to the A_2BX_4 group, with possible applications as transparent conductors, thin-film transistor materials, photovoltaic absorbers, and thermoelectrics. It leads to the prediction of 100 yet unreported A_2BX_4 compounds. Their lowest-energy crystal structures, formation enthalpies, and growth conditions were calculated. The emerging trends in stability and crystallography within the A_2BX_4 group of materials are discussed in the light of stable compounds predicted in this paper. A number of these A_2BX_4 compounds contain elements in their rare oxidation states, so avoiding the strong competition from competing

TABLE VI. Crystal structures and their total energies (in meV/atom) relative to the ground-state energy of Ti_2NiS_4, Cd_2PbO_4, Cd_2SnO_4, and Sc_2MgO_4.

Compound	Structure types (relative energies)											
Ti_2NiS_4	b5	b6	b7	b10	**d3**	S3I	b8	S3	b35	S2I	d3I	S2
	0	0	4	25	135	184	352	523	558	566	591	649
Cd_2PbO_4	b5I	**S3**	d3	b6	b7	b5	b36	S1I	b10I	S2I	S1	d3I
	0	206	428	431	431	435	440	454	472	474	499	501
Cd_2SnO_4	b5I	**S3**	b9I	d3	b35	S2I	S1I	S1	d3I	b5	b6	b7
	0	171	530	600	605	606	629	722	740	822	826	826
Sc_2MgO_4	b5	b7	b6	b10	b5I	S1	b38	S2	d3	b8	S3	**b9**
	0	0	0	215	253	279	504	620	638	706	739	962

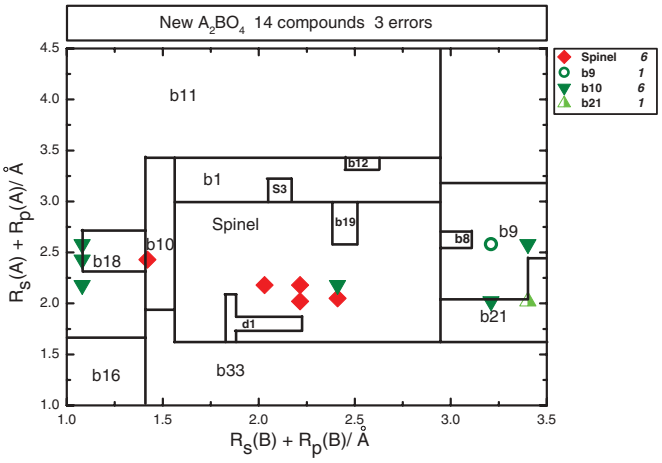

FIG. 9. (Color online) Orbital radii map for separation of structure types of the stable A_2BO_4 compounds predicted here.

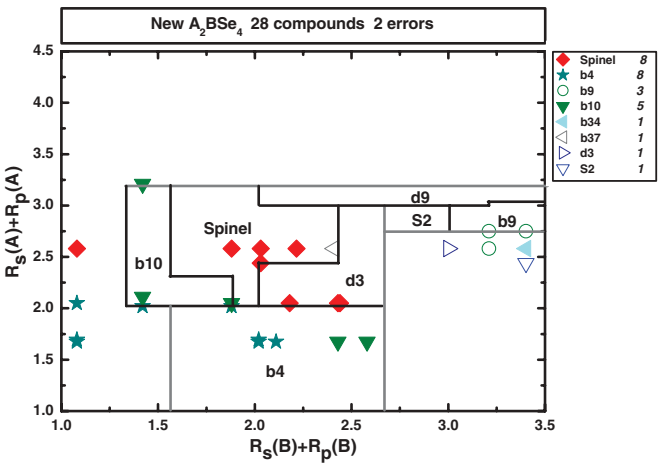

FIG. 11. (Color online) Orbital radii map for separation of structure types of the stable A_2BSe_4 compounds predicted here.

phases with elements in normal oxidation states. Our results emphasize the possibility of searching new materials in the wide arena of hypothetic compounds with elements in rare oxidation states. We suggest dozens of compounds that are not hard to synthesize with potentially game-changing material functionalities.

ACKNOWLEDGMENTS

This work was supported by the US Department of Energy, Office of Science, Basic Energy Sciences, Energy Frontier Research Centers, under Contract No. DE-AC36-08GO28308 to NREL. X.Z. also acknowledges the administrative support of REMRSEC at the Colorado School of Mines, Golden, Colorado, and thanks Lijun Zhang and Haowei Peng for helpful discussions. This research used resources of the National Energy Research Scientific Computing Center, which is supported by the Office of Science of the US Department of Energy under Contract DE-AC02-05CH11231 as well as capabilities of the National Renewable Energy Laboratory Computational Sciences Center, which is supported by the Office of Energy Efficiency and Renewable Energy of the US Department of Energy under Contract DE-AC36-08GO28308.

APPENDIX A: HIGHER-ENERGY STRUCTURES OF THE PREDICTED A_2BX_4 COMPOUNDS

The higher-energy crystal structures in the energy interval 100 meV/atom above the ground-state energies as well as ground-state structures of the 100 additional stable A_2BX_4 metal-chalcogenide compounds found in this paper are shown in Figs. 7 and 8. We are aware of the fact that for certain compounds (e.g., Sc_2HgS_4), some structure types (e.g., b6 and b7 distorted-spinel structures) can relax into their closely related structure type (e.g., b5 spinel structure) and have total energies (E_{tot}) very close to that of the latter structure. For consistency, we always assign the structure type with the lowest E_{tot} to be the lowest-energy structure.

Materials in higher-energy structures can sometimes be made in experiments, which may be the case of the four compounds (Ti_2NiS_4, Cd_2PbO_4, Cd_2SnO_4, and Sc_2MgO_4) that were assigned by orbital radii structure-field maps[6] to the structure types confirmed by first-principles calculations,

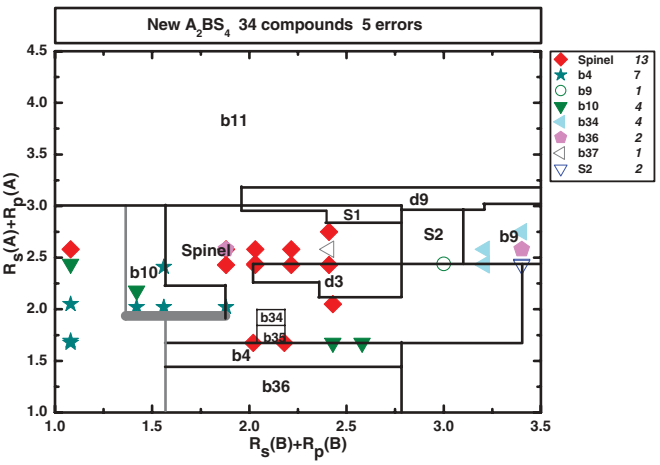

FIG. 10. (Color online) Orbital radii map for separation of structure types of the stable A_2BS_4 compounds predicted here.

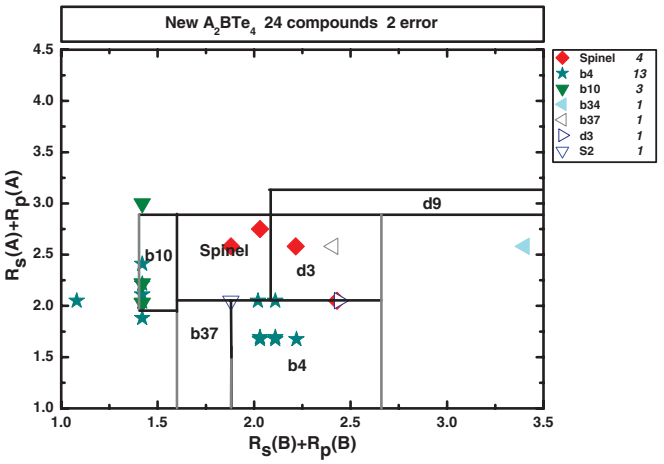

FIG. 12. (Color online) Orbital radii map for separation of structure types of the stable A_2BTe_4 compounds predicted here.

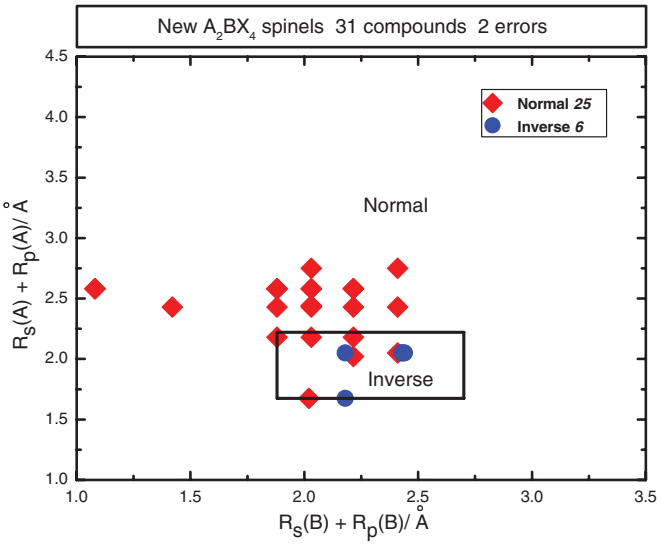

FIG. 13. (Color online) Orbital radii map for cation distribution of the stable spinel compounds predicted here.

while were found in experiments in other structures. Table VI lists the lowest-energy structure and 11 higher-energy structures of each of the four reported compounds (the structures found in experiments are in bold).

APPENDIX B: PREDICTIVE ABILITY OF ORBITAL RADII MAPS

The orbital radii maps constructed based on the information of known A_2BX_4 compounds (see Ref. 6) have been applied to the 100 stable A_2BX_4 compounds predicted here. The position of the border lines separating different structure types are the same as in Ref. 6. The gray border lines indicate the cases that the separation of existing A_2BX_4 compounds (see Ref. 6) does not require the position of these border lines to be fully invariable, i.e., they can be adjusted in certain ranges without creating more errors than those discussed in Ref. 6. We find 12 errors in total in Figs. 9–12 with a success rate of 88%, i.e., orbital radii maps assign them to be in the structure types other than those predicted by first-principles evaluation. They are: Ni_2BeO_4, Ti_2BaO_4, Ti_2BaS_4, Ti_2SnS_4, Al_2TiSe_4, Al_2VSe_4, Ni_2HgO_4, Sc_2BaS_4, Ti_2HgS_4, Ti_2SrS_4, Ti_2CdTe_4, and Ti_2HgTe_4. For the last six compounds, orbital radii maps give the second or third lowest-energy structure. We find two errors (Co_2CdO_4 and In_2HgO_4) in Fig. 13 with a success rate of 94%, i.e., orbital radii maps assign them to have cation distribution other than those predicted by first-principles evaluation.

*alex.zunger@gmail.com

[1] C. Wadia, A. P. Alivisatos, and D. K. Kammen, Environ. Sci. Technol. **43**, 2072 (2009).

[2] J. Akimoto, Y. Gotoh, K. Kawaguchi, and Y. Oosawa, J. Solid State Chem. **96**, 446 (1992).

[3] T. J. Coutts, D. L. Young, X. Li, W. P. Mulligan, and X. Wu, J. Vac. Sci. Technol. A **18**, 2646 (2000).

[4] M. Dekkers, G. Rijnders, and D. H. A. Blank, Appl. Phys. Lett. **90**, 021903 (2007).

[5] C. A. Hoel, T. O. Mason, J.-F. Gaillard, and K. R. Poeppelmeier, Chem. Mater. **22**, 3569 (2010).

[6] X. Zhang and A. Zunger, Adv. Funct. Mater. **20**, 1944 (2010).

[7] F. H. Allen, G. Bergerhoff, and I. Brown, *Crystallographic Databases* (International Union of Crystallography, Chester, 1987).

[8] A. Belsky, M. Hellenbrandt, V. L. Karen, and P. Luksch, Acta Crystallogr. Sect. B **58**, 364 (2002).

[9] ICDD PDF: International Centre for Diffraction Data, *Powder Diffraction File*, Newtown Square, Pennsylvania, USA.

[10] W. Setyawan and S. Curtarolo, Comput. Mater. Sci. **49**, 299 (2010).

[11] S. Curtarolo, D. Morgan, K. Persson, J. Rodgers, and G. Ceder, Phys. Rev. Lett. **91**, 135503 (2003).

[12] C. C. Fischer, K. J. Tibbetts, D. Morgan, and G. Ceder, Nat. Mater. **5**, 641 (2006).

[13] G. Hautier, C. C. Fischer, A. Jain, T. Mueller, and G. Ceder, Chem. Mater. **22**, 3762 (2010).

[14] T. Gruhn, Phys. Rev. B **82**, 125210 (2010).

[15] D. Kieven, R. Klenk, S. Naghavi, C. Felser, and T. Gruhn, Phys. Rev. B **81**, 075208 (2010).

[16] H.-J. Zhang, S. Chadov, L. Müchler, B. Yan, X.-L. Qi, J. Kübler, S.-C. Zhang, and C. Felser, Phys. Rev. Lett. **106**, 156402 (2011).

[17] A. Franceschetti and A. Zunger, Nature (London) **402**, 60 (1999).

[18] P. Piquini, P. A. Graf, and A. Zunger, Phys. Rev. Lett. **100**, 186403 (2008).

[19] R. G. Dandrea, J. E. Bernard, S.-H. Wei, and A. Zunger, Phys. Rev. Lett. **64**, 36 (1990).

[20] L. G. Wang and A. Zunger, Phys. Rev. Lett. **90**, 256401 (2003).

[21] G. Trimarchi and A. Zunger, Phys. Rev. B **75**, 104113 (2007).

[22] B. A. Wechsler and A. Navrotsky, J. Solid State Chem. **55**, 165 (1984).

[23] V. Stevanović, M. d'Avezac, and A. Zunger, J. Am. Chem. Soc. **133**, 11649 (2011).

[24] We use the Perdew-Burke-Ernzerhof (PBE) exchange-correlation functional[26] as implemented in the Vienna *ab initio* simulation package (VASP), the projector-augmented wave (PAW) pseudopotential,[27] energy cutoff of 220–520 eV. The reciprocal space is sampled using grids with densities of $2\pi \times 0.068$ and $2\pi \times 0.051$ Å^{-1} for relaxation and static calculations, respectively.

[25] For potentially magnetic compounds, we investigate several different starting magnetic configurations in the unit cell, including ferromagnetic, antiferromagnetic, and random spin configurations, initializing both high-spin and low-spin values on the transition metals, using a random algorithm. The spin configurations in big supercells are not tractable in the high-throughput way.

[26] J. P. Perdew, K. Burke, and M. Ernzerhof, Phys. Rev. Lett. **78**, 1396 (1997).

[27] G. Kresse and D. Joubert, Phys. Rev. B **59**, 1758 (1999).

[28] L. Wang, T. Maxisch, and G. Ceder, Phys. Rev. B **73**, 195107 (2006).

[29] S. Lany, Phys. Rev. B **78**, 245207 (2008).

[30]S. Lany, J. Osorio-Guillén, and A. Zunger, Phys. Rev. B **75**, 241203(R) (2007).

[31]V. Stevanović, S. Lany, X. Zhang, and A. Zunger, Phys. Rev. B **85**, 115104 (2012).

[32]S. L. Dudarev, G. A. Botton, S. Y. Savrasov, C. J. Humphreys, and A. P. Sutton, Phys. Rev. B **57**, 1505 (1998).

[33]W. M. C. Foulkes, L. Mitas, R. J. Needs, and G. Rajagopal, Rev. Mod. Phys. **73**, 33 (2001).

[34]At high temperature, one need to use the Gibbs free energy ($\Delta G = \Delta H - T\Delta S$) of the multinary compounds in the triangle analysis. The main entropy (S) effects in multinary compounds are vibrational entropy and configurational (e.g., cation disorder) entropy, which are comparably small relative to formation enthalpies.

[35]F. Ducastelle, *Order and Phase Stability in Alloys* (Elsevier Science, New York, 1991).

[36]S.-H. Wei, L. G. Ferreira, and A. Zunger, Phys. Rev. B **41**, 8240 (1990).

[37]Z. W. Lu, S.-H. Wei, A. Zunger, S. Frota-Pessoa, and L. G. Ferreira, Phys. Rev. B **44**, 512 (1991).

[38]S. Ping Ong, L. Wang, B. Kang, and G. Ceder, Chem. Mater. **20**, 1798 (2008).

[39]A. R. Akbarzadeh, V. Ozoliņš, and C. Wolverton, Adv. Mater. **19**, 3233 (2007).

[40]M. W. Finnis, Phys. Status Solidi A **166**, 397 (1998).

[41]S. B. Zhang, S.-H. Wei, A. Zunger, and H. Katayama-Yoshida, Phys. Rev. B **57**, 9642 (1998).

[42]T. R. Paudel, A. Zakutayev, S. Lany, M. d'Avezac, and A. Zunger, Adv. Funct. Mater. **21**, 4493 (2011).

[43]The fitted elemental energies were shown[31] to improve the ΔH_f values leading to the root-mean-square error of 0.07 eV/atom. Correspondingly, we repeat the triangle analysis for each compound ten more times varying the fitted elemental energy by -0.1 to 0.1 eV/atom. The compounds that can get both stable and unstable answers in the triangle analyses are labeled by undetermined in our accuracy of method.

[44]Selecting competing binary phases: we consider all known competing binary phases occurring in the known stoichiometries. The list we have of binary competing phases is rather rich and detailed and the likelihood that a structure of a binary chalcogenide will be missed is rather low. Selecting competing ternary phases: it is possible that a predicted A_2BX_4 compound will not be on a ground-state line because the sum of another missing ternary and known competing phases will be more stable. This is a limitation of our method. We partially protected against it by testing the triangle stability with respect to the following missing ternary phases with different stoichiometries: missing A_2BX_4 (A = Ti, B = Be, Mg, Ca, Sr, Ba, Zn, Cd, Hg, X = O, S, Se, Te) compounds as competing phases to A_2BX_4 (A = Be, Mg, Ca, Sr, Ba, Zn, Cd, Hg, B = Ti, X = O, S, Se, Te), and vice versa. We found that adding the missing ternary compounds does not change the stability $\Delta\mu_I$ regions at all.

[45]A. Vaipolin, Y. Nikolaev, I. Polushina, V. Rud', Y. Rud', E. Terukov, and N. Fernelius, Semiconductors **37**, 641 (2003).

[46]G. Doll, A. Anghel, J. R. Baumann, E. Bucher, A. P. Ramirez, and K.-J. Range, Phys. Status Solidi A **126**, 237 (1991).

[47]W. P. F. A. M. Omloo, J. C. Bommerson, H. H. Heikens, H. Risselada, M. B. Vellinga, C. F. van Bruggen, C. Haas, and F. Jellinek, Phys. Status Solidi A **5**, 349 (1971).

[48]J. Jumas, M. Ribes, E. Philippot, M. Maurin, C. R. Acad. Sc. Paris C **284**, 845 (1977).

[49]The structure-search with GSGO was performed for structures with less than 28 atoms. The population size is set to 64 and the 16 worst individuals are replaced by offspring at each generation. The rate of crossover versus mutation is set to 0.7. A minimum of two independent evolutionary runs with 12 or more generations are performed for each GSGO search.

[50]J. Osorio-Guillén, S. Lany, S. V. Barabash, and A. Zunger, Phys. Rev. Lett. **96**, 107203 (2006).

[51]R. W. G. Wyckoff, *Crystal Structures* (Krieger Publishing, Malabar, Florida, 1981), Vols. 2 and 3.

[52]A. Zunger, Phys. Rev. B **22**, 5839 (1980).